REPORT DOCUMENTATION PAGE

AFRL-SR-BL-TR-02-

$\mathcal{OO64}$

1. AGENCY USE ONLY *(Leave blank)*	2. REPORT DATE	3. REPO .... DATES COVERED
	14 Feb 02	FINAL REPORT 01 Nov 97 - 31 Oct 00

4. TITLE AND SUBTITLE
THEORETICAL DETERMINATION OF OPTIMIZED STRUCTURES FOR
MOLECULAR COMPLEXES AND CLUSTERS

5. FUNDING NUMBERS
F49620-98-1-0082

3484/BS

61103D

6. AUTHOR(S)
Dr Peter Pulay and Dr Jon Baker

7. PERFORMING ORGANIZATION NAME(S) AND ADDRESS(ES)
University of Arkansas
Department of Chemistry and Biochemistry
Fayetteville AR 72701

8. PERFORMING ORGANIZATION REPORT NUMBER

9. SPONSORING/MONITORING AGENCY NAME(S) AND ADDRESS(ES)
AFOSR/NL
801 Randolph St., Room 732
Arlington, VA 22203-1977

10. SPONSORING/MONITORING AGENCY REPORT NUMBER

11. SUPPLEMENTARY NOTES

AIR FORCE OFFICE OF SCIENTIFIC RESEARCH (AFOSR)
NOTICE OF TRANSMITTAL DTIC. THIS TECHNICAL REPORT
HAS BEEN REVIEWED AND IS APPROVED FOR PUBLIC RELEASE
LAW AFR 190-12. DISTRIBUTION IS UNLIMITED.

12a. DISTRIBUTION AVAILABILITY STATEMENT

DISTRIBUTION STATEMENT A
Approved for Public Release
Distribution Unlimited

12b. DISTRIBUTION CODE

13. ABSTRACT *(Maximum 200 words)*
Our original proposal was in two parts. The first involved improved optimization methods for clusters and weakly interacting systems. Traditional optimization methods do not take into account the special character of these systems, such as the large disparity between the forces within and between molecules, and are thus inefficient. Our aim here was to develop an efficient optimization procedure for weakly interacting molecular clusters, as well as for other non-standard optimization scenarios, such as molecular adsorption on a model surface. The second project dealt with improved electronic structure methods for large molecular systems. The main thrust here was the development of efficient algorithms for the computation of both canonical and local MP2 energies and gradients. Current density functionals are not able to adequately model dispersion forces and MP2 should be a good option here. These latter calculations can eventually supply molecular energies and gradients for the optimization project. We have also developed a preliminary version of an atom-centered fast multipole program for large-molecule DFT calculations.

14. SUBJECT TERMS

16. PRICE CODE

17. SECURITY CLASSIFICATION OF REPORT	18. SECURITY CLASSIFICATION OF THIS PAGE	19. SECURITY CLASSIFICATION OF ABSTRACT	20. LIMITATION OF ABSTRACT

FINAL PROGRESS REPORT TO THE AIR FORCE OFFICE OF SCIENTIFIC RESEARCH

THEORETICAL DETERMINATION OF OPTIMIZED STRUCTURES FOR MOLECULAR COMPLEXES AND CLUSTERS

Peter Pulay and **Jon Baker**

Department of Chemistry and Biochemistry
University of Arkansas
Fayetteville
Arkansas 72701

INTRODUCTION

Our original proposal was in two parts. The first involved improved optimization methods for clusters and weakly interacting systems. Traditional optimization methods do not take into account the special character of these systems, such as the large disparity between the forces within and between molecules, and are thus inefficient. Our aim here was to develop an efficient optimization procedure for weakly interacting molecular clusters, as well as for other non-standard optimization scenarios, such as molecular adsorption on a model surface.

The second project dealt with improved electronic structure methods for large molecular systems. The main thrust here was the development of efficient algorithms for the computation of both canonical and local MP2 energies and gradients. Current density functionals are not able to adequately model dispersion forces and MP2 should be a good option here. These latter calculations can eventually supply molecular energies and gradients for the optimization project. We have also developed a preliminary version of an atom-centered fast multipole program for large-molecule DFT calculations.

This final report summarizes the progress made in these areas during the period of this grant award. No great detail is given, as this has to a large extent already been provided in our previous yearly reports.

1. Optimization of Molecular Geometries

a. Cluster and Rigid-Body Optimization

We have successfully developed and fully implemented an algorithm for the efficient optimization of molecular clusters. This uses a special set of what we have called *cluster coordinates*, which comprise the usual stretches, bends and torsions to describe the interactions *within* each molecule (the intramolecular geometry) and inverse-distance coordinates to describe the interactions *between* individual molecules in the cluster (the intermolecular geometry). Our new cluster coordinates reduce the number of geometry optimization cycles required for convergence by up to an order of magnitude relative to Cartesian coordinates, and also significantly relative to other coordinates, e.g., distance coordinates. Molecular clusters usually have a number of minima, and cluster coordinates are often more successful in reaching low-lying minima than are Cartesians.

In addition, by using a Schmidt-Orthogonalization scheme for imposing constraints introduced earlier (J.Baker, A.Kessi and B.Delley, *J.Chem.Phys.* **105** (1996) 192), it is possible to effectively constrain all the intramolecular degrees of freedom in a molecular cluster and in this way carry out complete rigid-body optimizations.

We illustrate the efficacy of our new cluster coordinates by optimizing the geometries of twenty randomly-generated clusters, each containing ten hydrogen molecules. Table 1 shows the starting energy, the number of optimization cycles needed to converge and the final energy for optimizations using both Cartesian and cluster coordinates. As can

2

be seen, the average rate of convergence is over ten times faster with cluster coordinates than with Cartesians, and in each case the optimization converged to a lower final energy.

Table 1
Starting energy, number of cycles to converge and final energy for the RHF/3-21G optimization of 20 randomly generated clusters of 10 H_2 molecules (initial bond length 0.72 Å)

cluster	starting energy	Cartesian		cluster coordinates[a]	
		cycles	energy[b]	cycles	energy[b]
1	-11.166613	613	-11.230147	34	-11.230188
2	-11.151158	506	-11.230130	33	-11.230208
3	-11.159068	282	-11.230023	30	-11.230193
4	-11.142043	100	-11.229742	55	-11.230162
5	-11.177657	776	-11.230133	24	-11.230170
6	-11.178220	305	-11.229987	58	-11.230176
7	-11.150748	338	-11.230103	31	-11.230226
8	-11.152618	410	-11.230122	47	-11.230212
9	-11.170617	454	-11.230144	17	-11.230226
10	-11.148964	425	-11.230093	42	-11.230196
11	-11.157261	431	-11.230073	70	-11.230190
12	-11.171696	501	-11.230054	39	-11.230223
13	-11.161546	500	-11.230130	66	-11.230223
14	-11.164816	435	-11.230041	33	-11.230176
15	-11.143458	478	-11.230110	32	-11.230226
16	-11.151136	965	-11.230106	54	-11.230208
17	-11.157329	555	-11.230116	33	-11.230206
18	-11.171771	357	-11.230074	41	-11.230190
19	-11.141685	172	-11.229711	39	-11.230206
20	-11.150264	307	-11.230016	35	-11.230202
average		**446**	**-11.230053**	**41**	**-11.230200**

[a] intermolecular cluster coordinates were based on simple inverse distances (1/R)

[b] convergence criteria were a maximum gradient component < 0.00005 au and an energy change of < 10^{-7} hartree

b. Geometry Optimization for Reactions on Model Surfaces

We have developed an efficient and automatic procedure for optimizing the geometries of surface-adsorbate systems. Internal coordinates (stretches, bends and torsions) are generated for the surface and the molecule being adsorbed separately, and additional linking primitives are generated to connect the two parts. The often high atomic connectivity in the model surface makes it possible to ignore torsions, spanning all surface degrees of freedom using stretches and bends only, greatly reducing the dimension of the primitive space. Cartesian coordinates (i.e., fixed atoms) can be constrained within a delocalized internal coordinate optimization (by constraining all primitives that involve solely the fixed atoms in their definition), and the effects of freezing various surface layers on reaction energetics and geometries can be investigated.

We have used this procedure to investigate the dissociative adsorption of water on the reactive site of the silicon (100) surface, modelled using Si_9H_{12} and $Si_{17}H_{20}$ clusters (see Fig. 1). The Si atoms labelled 1 and 2 in both cases constitute the "active site" and these two atoms are formally unsaturated. They are considered to be in the first (or surface) layer in our model. Si atoms 3, 4, 5 and 6 comprise the second layer. All other Si atoms are taken as the third layer. Apart from the two surface atoms, the remaining Si atoms are saturated by adding hydrogens.

The reaction is considered to take place by first forming a complex between water and the Si surface, with a bond forming between the water oxygen and, say, Si atom 1, with Si atoms 1 and 2 and the water molecule all in the same plane; this is followed by a lengthening of one of the water O-H bonds and the partial formation of a Si-H bond with Si atom 2 (in the transition state), leading to the final product with the water molecule completely dissociated and full Si-OH and Si-H bonds at the previously unsaturated Si centers.This process is shown schematically in Fig. 2. By systematically fixing Si atoms (and their attached hydrogens) in the three surface "layers" defined above, we can investigate the effects on the reaction energetics of freezing various surface layers.

Reaction energetics are shown in Table 2. We used density functional theory (specifically the hybrid B3LYP functional with the standard 6-31G* basis set). All structures were taken to be closed shell singlets. The initial geometries of both Si_9H_{12} and $Si_{17}H_{20}$ were fully optimized at B3LYP/6-31G*.
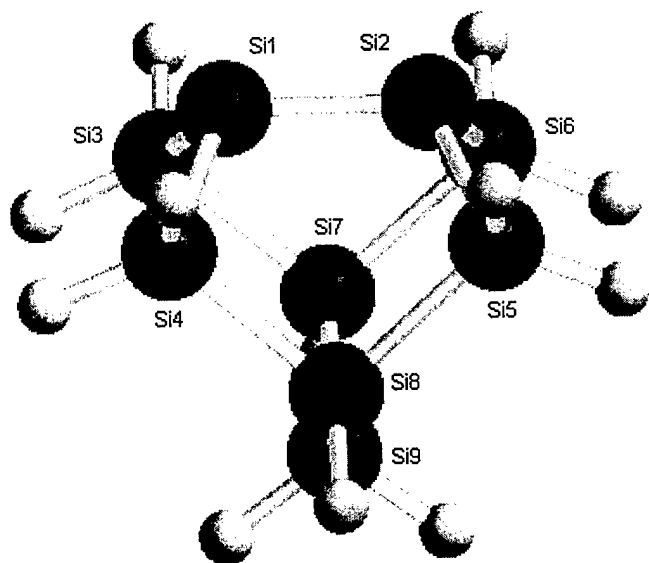
Figure 1a: Structure of Si_9H_{12}
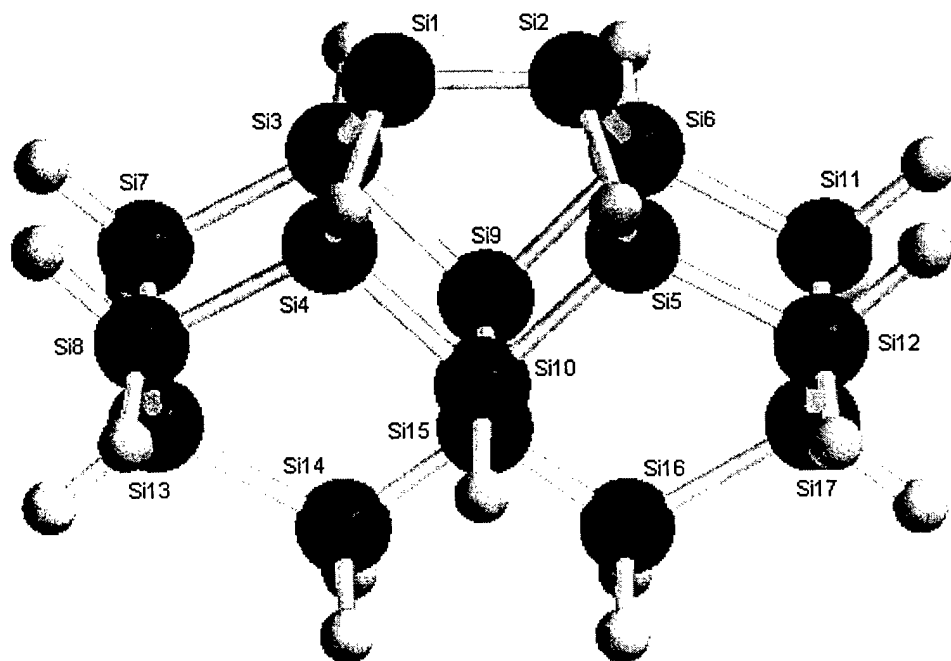

Figure 1b: Structure of $Si_{17}H_{20}$

Table 2 Energetics of the dissociative adsorption reaction ($H_2O \longrightarrow H + OH$) on the model Si_9H_{12} and $Si_{17}H_{20}$ surfaces (in kcal/mol relative to the initial adsorbed complex as the energy zero)

surface type	$Si_9H_{12} + H_2O$	$H_2O\text{-}Si_9H_{12}$	transition state	$Si_9H_{13}OH$
fixed surface	+5.3	0.0	+3.1	-53.0
layer 1 free	+11.7	0.0	+4.0	-53.8
layers 1 & 2 free	+14.4	0.0	+5.3	-52.3
unconstrained	+14.9	0.0	+5.5	-53.0

surface type	$Si_{17}H_{20} + H_2O$	$H_2O\text{-}Si_{17}H_{20}$	transition state	$Si_{17}H_{21}OH$
fixed surface	+5.8	0.0	+2.8	-53.1
layer 1 free	+12.9	0.0	+4.0	-53.8
layers 1 & 2 free	+15.1	0.0	+5.1	-52.4
unconstrained	+15.8	0.0	+5.1	-52.7

As can be seen from Table 2, the effect on the overall relative energetics of freezing various surface layers is minor. The initial binding between water and the model surface is fairly strong systematically increases with increasing surface relaxation; this must be the case as we are comparing fully optimized reactants with only a partially optimized complex - relaxation of each surface layer can only lower the energy of the complex, thus increasing the binding. However, the relative energy difference between the adsorbed complex, the transition state, and the dissociatively adsorbed product, hardly differs as we systematically relax the surface. The only real trend is a small but steady increase in the transition state barrier with increasing surface relaxation. The energetics on the totally frozen compared to the totally relaxed surface are very similar, as are the results for the $Si_{17}H_{20}$ cluster compared to Si_9H_{12}.

Given the quality of the calculations (a reasonable but not especially high level of theory), our conclusions are: (1) that the frozen surface model provides a pretty good picture of the overall reaction energetics; and (2) that the Si_9H_{12} model surface seems to be perfectly adequate to describe the dissociative adsorption of a water molecule on a silicon cluster.

6

Figure 2: Schematic of geometrical arrangement around the active site for the dissociative adsorption of water on a model Si (100) surface for: (a) the initial adsorbed complex; (b) the transition state; (c) the dissociatively adsorbed product (see Table 1)
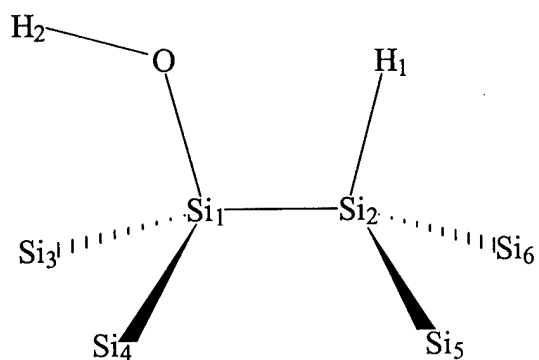
(a)
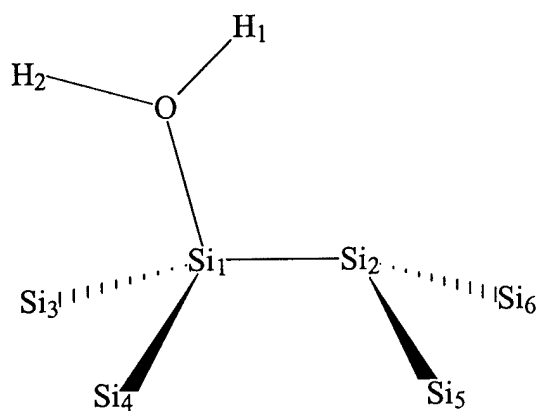
(b)
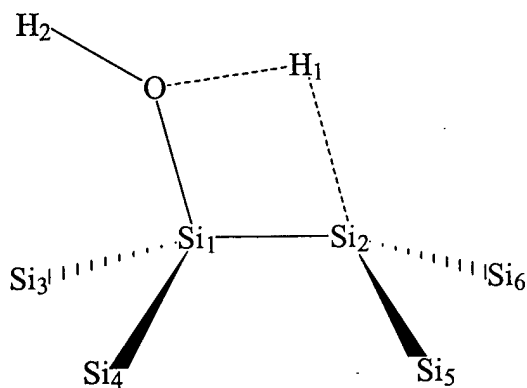
(c)

c. Large-Molecule Optimization

The bottleneck preventing the efficient use of internal coordinates in large systems is the time taken to transform the gradient (and possibly the Hessian) from Cartesian coordinates to internal coordinates, and to transform the new geometry from internal coordinates back to Cartesians. The latter step is needed to calculate the energy and gradient for the next optimization step. Both these transformation steps formally scale as the cube of the system size, $O(N^3)$. We have developed several novel algorithms to reduce this scaling to near-linear.

The gradient transformation can formally be written as

$$g^{cart} = B^t g^{int} \qquad (1)$$

where B is the (linearized) transformation matrix from Cartesian to internal coordinates (the so-called Wilson B-matrix). As it is not a square matrix, B^t does not have a regular inverse, and the usual trick is to define $(B^t)^{-1} = (BB^t)^{-1}B$, which acts as a left inverse in the sense that $(B^t)^{-1}B^t = 1$. The cubic computational dependence of traditional internal coordinate transformations is caused by the presence of this formal matrix inverse.

Using this left inverse we can write

$$g^{int} = (B^t)^{-1} g^{cart} = (BB^t)^{-1}B \, g^{cart} \qquad (2)$$

which can be rearranged to

$$(BB^t) g^{int} = B \, g^{cart} \qquad (3)$$

Splitting off the diagonal D of BB^t, we can rewrite eq. 3 as

$$D g^{int} = B \, g^{cart} + (D - BB^t) g^{int} \qquad (4)$$

and convert it into an iterative scheme

$$g^{int}(k+1) = D^{-1} [B \, g^{cart} + (D - BB^t) g^{int}(k)] \qquad (5)$$

which can be solved by the preconditioned conjugate gradient method. Solution of Eq. 5 is formally $O(N^2)$ as it no longer contains a matrix inverse. In practice, however, the actual order depends on how rapidly the procedure converges; if it takes $O(N)$ cycles to converge, then nothing is gained.

The backtransformation of the new geometry from internal to Cartesian space is also accomplished iteratively via

$$x(k+1) = x(k) + (B^t)^{-1}(k) [q - q(k)] \qquad (6)$$

Here q is the (known) new geometry in internal coordinates and the iterative procedure is typically started (k=1) using the *old* Cartesian geometry (and the old B matrix). Although this iterative back transformation normally converges extremely rapidly (differences between q and $q(k)$ of $< 10^{-10}$ in 3-5 cycles), it formally requires the construction and inversion of a new B matrix at *each* iterative cycle. A better scheme, which works unless the displacements are very large, is to keep the old $(B^t)^{-1}$ matrix throughout; this increases the number of cycles but each cycle is now much less expensive as no matrix inverse is needed.

Our first approach involved direct solution of Eq. 2 using natural internal coordinates and a scheme in which the formal inverse of BB^t is replaced by the inverse of its approximate symmetric Cholesky decomposition LdL^t, where L is lower triangle and d is diagonal. In the decomposition, we keep only elements of L that exceed a small threshold; this number is expected to grow approximately linearly with system size. This reduces the gradient transformation to roughly $O(N^2)$; it also has the advantage that the *same* decomposition can be used for the backtransformation, Eq. 6 (assuming that the geometry change is not too large).

We subsequently developed an alternative approach using delocalized internal coordinates and the iterative gradient transformation of Eq. 5. Delocalized internals are formed by diagonalization (or its equivalent) of BB^t on the first optimization cycle and, after transformation to the new coordinate space, the BB^t matrix is usually diagonally dominant throughout the optimization. This ensures that Eq. 5 converges rapidly. However, the main advantage of delocalized internals is that the formal $O(N^3)$ traditional backtransformation can be replaced by a Z-matrix approach which is $O(N)$. (This Z-matrix backtransformation cannot readily be used with natural internals because they mix in too much of the formally redundant part of the full space of primitive internals.) Unfortunately, delocalized internals - being linear combinations of all possible stretches, bends and torsions in the primitive space (unlike natural internals, which are linear combinations of just a few primitives and are highly localized) - are not efficient beyond a certain molecular size (around 500 or so atoms) due to their lack of sparsity. Natural internals *are* sparse, but are increasingly difficult to generate as molecular size and topological complexity increases.

Our most recent approach is capable of carrying out large-molecule geometry optimizations directly in the *full* space of primitive internal coordinates. Normally far more primitive stretches, bends and torsions can be generated for a large molecule containing N atoms than the 3N-6 that are necessary to span all the internal degrees of freedom. Although the B matrix in primitive internals can have a much greater dimension than, say, its equivalent in delocalized internals, it is highly sparse, having at most 12 non-zero entries per column regardless of the number of primitives, which could easily be in the tens of thousands for a system with a few thousand atoms. If we let $g^{int} = Bx$, then substituting into Eq. 1 gives

$$g^{cart} = B^tB x \tag{7}$$

We can solve this set of linear equations to get x, and then back-substitute to get g^{int}. This involves the formal inverse of B^tB (instead of BB^t), and not only does this matrix have smaller dimension than BB^t (3N-6 instead of the size of the primitive space), but it turns out that its approximate Choleskly decomposition has a sparser L matrix than for the corresponding BB^t matrix, leading to a further reduction in CPU time for the transformation.

To give some idea of the efficiency of our coordinate transformations, and the

performance of the optimization overall, we present the following three Tables. Table 3 shows timings for various steps in the large-molecule, delocalized internal coordinate algorithm, together with the timings (old) if all transformations were done using full matrix inversions.

Table 3

Timings (CPU; seconds) on an IBM RS6000/390 workstation for various steps in the internal-coordinate large-molecule optimization algorithm.

cycle[a]	B Matrix[b] construction		gradient[c] transformation		back[c] transformation		total time	
	old	new	old	new	old	new	old	new
Jawsamycin ($C_{32}H_{43}N_3O_6$, 84 atoms)								
1	34.01	12.61	2.01	0.03	16.54	0.12	53.41	13.61
2	2.09	0.27	2.03	0.10	16.54	0.14	20.68	0.53
3	2.12	0.27	2.02	0.12	16.54	0.17	20.70	0.58
30	2.12	0.27	2.01	0.55	12.37	0.23	16.52	1.07
Taxol ($C_{47}H_{51}NO_{14}$, 113 atoms)								
1	110.06	23.09	4.46	0.05	36.19	0.23	152.24	24.90
2	4.57	1.45	4.41	0.22	36.15	0.25	45.17	1.96
3	4.58	1.45	4.41	0.22	36.15	0.25	45.18	1.96
68	4.59	1.44	4.46	1.36	27.10	0.98	36.19	3.82
(Alanine)$_{20}$ ($C_{60}H_{102}N_{20}O_{21}$, 203 atoms)								
1	826.07	97.25	99.91	0.29	492.97	0.42	1439.47	118.48
2	23.71	9.30	99.96	1.07	626.28	0.51	750.13	11.06
3	23.80	9.27	100.01	1.42	620.58	0.51	744.57	11.38
63	23.80	9.29	100.37	2.50	372.89	0.58	497.24	12.55

[a] Shown are timings for the first three optimization cycles and the final cycle. Convergence criteria are: maximum gradient component < 0.00005 E_h/a_0; energy change < 10^{-7} E_h

[b] Timings for B matrix construction on cycle 1 include once only construction of delocalized internals

[c] The fast gradient and back transformation were converged to an accuracy of better than 5×10^{-9}

As can be seen, the savings are enormous even for these relatively small systems. Our most recent B^tB algorithm, using either natural internal coordinates or a full set of primitive internals, is even faster for all steps except possibly the backtransformation. Table 4 shows timings for the gradient transformation and the total (average) time per optimization cycle for a series of alanine polypeptides; also shown are the density (the percentage of non-zero elements) in the Cholesky decomposition for both the B^tB and the original BB^t algorithm.

Table 4. Comparison of the performance of the B^tB and BB^t formalisms for alpha-helical alanine polypeptides. The following data are shown: the density (the fraction of non-zero elements) in the Cholesky factors, and the average time (T_{cycle}, sec) per optimization cycle (a few decompositions, one force transformation, and a line search including 4-5 geometry back-transformations) on a 300 MHz Pentium II PC for both the B^tB and BB^t formalisms. For the B^tB formalism the average time (T_{Force}, sec) of a single force transformation step is also shown.

Alanine polypeptides		B^tB			BB^t	
# of alanine units	# of atoms	Density %	T_{Force}	T_{cycle}	Density %	T_{cycle}
10	109	17.95	0.05	0.77	26.37	1.09
20	209	9.63	0.11	1.61	18.86	2.70
30	309	6.58	0.21	2.62	13.20	5.21
40	409	4.99	0.24	3.88	10.77	8.24
50	509	4.02	0.37	5.23	9.32	12.29
100	1009	2.04	0.70	11.17	5.94	40.04
200	2009	1.03	1.33	22.74	3.88	137.97
300	3009	0.69	2.01	32.28	-	-
500	5009	0.41	2.49	49.55	-	-
700	7009	0.30	3.40	71.45	-	-
999	9999	0.21	4.57	91.62	-	-

Finally Table 5 directly compares the performance of our large-molecule internal coordinate optimization algorithm with the standard conjugate gradient optimizer in Cartesian coordinates in the TINKER molecular mechanics package (J.W.Ponder, *Software Tools for Molecular Design*, version 3.7, June 1999) for the same alanine polypeptides shown in Table 4. As can be seen, our algorithm converges in dramatically fewer energy and gradient evaluations than the more traditional Cartesian optimizer and typically converges to a lower final energy. This is particularly apparent for the larger systems.

Table 5 Comparison of optimizations of alpha-helical alanine polypeptides using natural internal and Cartesian coordinates. The initial and final energies (kcal/mol) and the number of gradient and energy evaluations are shown for Cartesian optimizations as implemented in the TINKER program (*minimize.x*) and natural internal coordinate optimizations in our program

# of alanines	initial energy	Natural Internal Coordinates			TINKER (0.01 kcal/mol Å)		
		# of		final energy	# of		final energy
		E	G		E	G	
10	11.4867	31	138	-43.3114	313	578	-43.3124
20	6.2427	38	168	-97.4764	412	770	-97.4768
30	0.7077	50	216	-152.1734	354	675	-152.1717
40	-4.8271	53	237	-206.8709	335	636	-206.8696
50	-10.3619	64	314	-261.5697	436	797	-261.5688
100	-38.0366	71	340	-535.0629	664	1246	-535.0583
200	-427.7795	69	336	-1082.0471	1589	3020	-1081.9656
300	-650.1882	76	368	-1629.0323	2191	4051	-1628.7909
500	-2630.4851	48	234	-2723.0002	6369	12228	-2719.7795
700	-3688.1297	50	244	-3816.9708	6536	12614	-3799.8068
999	-5269.9224	55	267	-5452.4565	7851	15165	-5414.0775

12

II. Electronic Structure Theory

a. Local Electron Correlation

We have continued developing our local second-order Møller-Plesset perturbation theory code.

<This part to be completed by PP>

b. Atom-centered fast multipoles

The aim of this research project is to develop a fast and accurate DFT program for large molecules. Instead of calculating all the two-electron integrals as in the traditional quantum chemical approach, we expand the Coulomb potential in terms of spherical harmonics over atom-centered grids. Our approach is similar to that of Delley in the DMol program (B.Delley, *J.Chem.Phys.* **92** (1990) 508), except that we subsequently fit the *potential* rather than do a global fit to the *density* as is the case in DMol. In large molecules, the Coulomb potential between atoms that are far apart can be described by a simple multipole expansion, and this is where we hope to gain efficiency over the more traditional methods. Our approach is conceptually similar to the Continuous Fast Multipole Expansion (C.A.White, B.G.Johnson, P.M.W.Gill and M.Head-Gordon, *Chem.Phys.Lett.* **230** (1994) 8). However, in CFMM the molecule is divided into artificial rectangular boxes, with multipole expansions being used to describe the Coulomb interactions between boxes that are far enough apart. These rectangular boxes require high order multipoles and are responsible for the fact that CFMM becomes really efficient only for huge systems. Our approach, with spherical atom-centered expansions, is more physical and expected to give a crossover with traditional methods at much smaller system size.

Initially we have concentrated on producing accurate and reliable DFT energies for small and medium-sized molecules and have, we believe, obtained some of the most accurate energies using this approach that have been reported to date. We have been very careful with our numerical integration techniques, and can take the various expansions involved to high orders in spherical harmonics to reach limiting values. Using identical Gaussian basis sets, we can directly compare energies from the fully numerical spherical harmonics code with energies from traditional quantum chemistry DFT codes to determine how high to take L in the spherical harmonics expansion to accurately reproduce traditional DFT energies. Our findings suggest that high values of L are needed even to reproduce relative energies accurately, and that the default expansions in many commonly used codes are probably too low to give reliable energetics.

Table 6 shows energies for a number of di- and tri-atomics for L values in the spherical harmonics expansion from 0 to 19. For most of the molecules investigated, absolute energies do not stabilize until at least L=11 and for some, e.g. F_2, not even then.

Table 6 Analytical and numerical BLYP/6-31G** SCF energies (hartree) for a number of small molecules for L values in the spherical harmonic expansions from 0 to 19

L_{max}	H_2	LiH	HF	Li_2	LiF
0	-1.159720	-8.099536	-100.552673	-15.158289	-108.390760
1	-1.156331	-8.070451	-100.321579	-14.965681	-107.743656
2	-1.166369	-8.068231	-100.376894	-14.979977	-107.459285
3	-1.168114	-8.064447	-100.409630	-14.991192	-107.380373
4	-1.168037	-8.064419	-100.414410	-14.994298	-107.371944
5	-1.167918	-8.066075	-100.412624	-14.993896	-107.382928
6	-1.167889	-8.066663	-100.411409	-14.993019	-107.393007
7	-1.167888	-8.066573	-100.411075	-14.992559	-107.398321
8	-1.167890	-8.066523	-100.411025	-14.992445	-107.400443
9	-1.167890	-8.066545	-100.411029	-14.992465	-107.401152
10	-1.167890	-8.066544	-100.411050	-14.992502	-107.401342
11	-1.167890	-8.066533	-100.411075	-14.992524	-107.401334
12	-1.167890	-8.066531	-100.411078	-14.992527	-107.401307
13	-1.167890	-8.066531	-100.411080	-14.992527	-107.401258
14	-1.167890	-8.066530	-100.411079	-14.992527	-107.401204
15	-1.167890	-8.066530	-100.411079	-14.992527	-107.401158
16	-1.167890	-8.066530	-100.411079	-14.992527	-107.401126
17	-1.167890	-8.066530	-100.411079	-14.992527	-107.401107
18	-1.167890	-8.066530	-100.411079	-14.992527	-107.401100
19	-1.167890	-8.066530	-100.411079	-14.992527	-107.401098
no pruning*	-1.167891	-8.066535	-100.411094	-14.992534	-107.400661
exact	**-1.167896**	**-8.066464**	**-100.411080**	**-14.992538**	**-107.400627**

Table 6 (continued)

L_{max}	CO	N_2	F_2	H_2O	CO_2
0	-112.815305	-108.970494	-199.188346	-76.444437	-187.634789
1	-113.259613	-109.387299	-199.355946	-76.249007	-188.254279
2	-113.207833	-109.412242	-199.500291	-76.365904	-188.444913
3	-113.269420	-109.490394	-199.476625	-76.404018	-188.490216
4	-113.292217	-109.512858	-199.480261	-76.403080	-188.569540
5	-113.296366	-109.515300	-199.488192	-76.399434	-188.566628
6	-113.295616	-109.513217	-199.492640	-76.398689	-188.566551
7	-113.294325	-109.511063	-199.493785	-76.398819	-188.565544
8	-113.293430	-109.509823	-199.493646	-76.398901	-188.563028
9	-113.292972	-109.509398	-199.493387	-76.398906	-188.563087
10	-113.292799	-109.509394	-199.493261	-76.398917	-188.562201
11	-113.292770	-109.509498	-199.493201	-76.398933	-188.562271
12	-113.292775	-109.509517	-199.493181	-76.398935	-188.562270
13	-113.292783	-109.509524	-199.493160	-76.398934	-188.562268
14	-113.292787	-109.509525	-199.493146	-76.398934	-188.562287
15	-113.292789	-109.509525	-199.493139	-76.398933	-188.562287
16	-113.292790	-109.509524	-199.493138	-76.398933	-188.562290
17	-113.292790	-109.509524	-199.493139	-76.398932	-188.562291
18	-113.292789	-109.509524	-199.493142	-76.398932	-188.562290
19	-113.292789	-109.509524	-199.493143	-76.398932	-188.562290
no pruning*	-113.292929	-109.509526	-199.492959	-76.398934	-188.562392
exact	**-113.292888**	**-109.509547**	**-199.492937**	**-76.398886**	**-188.562330**

* the various atom-centered grids are normally "pruned" to reduce the number of angular grid points in appropriate regions of space, e.g., close to the nucleus; "no pruning" energies are with the full grid without any reduction in the number of angular grid points.

To give some idea as to the relative accuracy of our fully numerical DFT energies we note that Becke and Dickson have taken L up to 11, but their reported energy for, e.g., CO_2 (see Table II in A.D.Becke and R.M.Dickson, *J.Chem.Phys.*, **89** (1988) 2993) deviates by 0.016 hartree from the exact value, compared to our error of 0.000062 hartree (Table 6). The current default in DMol is L = 4.

3. Other Projects

In addition to our two major research topics, a number of other research projects in the Pulay group have been supported from our Air Force grant.

- We have implemented a new Gaussian-weighted operator, originally developed by Rassolov and Chipman for MCSCF wavefunctions (V.A.Rassolov and D.A.Chipman, *J.Chem.Phys.* **105** (1996) 1470), for the calculation of spin densities at nuclei in density functional theory. Applications to first row atoms and some diatomic and small polyatomic molecules show good agreement with experiment.

- We have carried out a thorough investigation into the inner-hydrogen migration and ground-state structure of porphycene (a structural isomer of porphyrin). We were able to convincingly show via good quality density functional calculations and an SQM force field analysis of the vibrational spectrum, that the ground-state structure is the C_{2h} *trans* isomer and a previously proposed scheme for the inner-hydrogen migration involving both the *trans* and *cis* isomers was not viable.

- We have investigated the structure and IR spectra of a number of metal tris-acetylacetonates, correcting some of the experimental assignments and predicting the geometry and vibrational spectrum of several species (e.g., the scandium compound) which, to our knowledge, have not been experimentally determined. Excellent agreement was obtained with experimental IR spectra for the Al, Fe and Cr compounds.

Personnel Supported

Jon Baker	Co-P.I. (50% appointment)
Peter Pulay	P.I. (2 month)
Roberto Lopez Boada	Post-Doctoral Associate (1 year)
Svein Saebo	Visiting Faculty (18 weeks)
Bela Paizs	Visiting Scientist (6 weeks)
Irina Diaz-Acosta	Graduate Student (partial support)
Bing Wang	Graduate student (partial support)

The work discussed in this final report has been published in the following scientific journals:

1. A. El-Azhary, G. Rauhut, P. Pulay and H-J. Werner, *Analytical Energy Gradients for Local Second-Order Moller=Plesset Perturbation Theory*,
    J. Chem. Phys. **108** (1998) 5185

2. G. Hetzer, P. Pulay and H-J. Werner, *Multipole Approximation of Distant Pair Energies in Local MP2 Calculations*, Chem. Phys. Lett. **290** (1998) 143

3. M. Kozlowski, M. Z. Zgierski and J. Baker, *The Inner-Hydrogen Migration and Ground-State Structure of Porphycene*, J. Chem. Phys. **109** (1998) 5905

4. J. Baker, D. Kinghorn and P. Pulay, *Geometry Optimimization in Delocalized Internal Coordinates: An Efficient Quadratically Scaling Algorithm for Large Molecules*, J. Chem. Phys. **110** (1999) 4986

5. J. Baker and P. Pulay, *Efficient Geometry Optimization of Molecular Clusters*,
    J. Comput. Chem. **21** (2000) 69

6. B. Wang, J. Baker and P. Pulay, *Density Functional Implementation of a Gaussian-Weighted Operator for Spin Densities*,
    Phys. Chem. Chem. Phys. **2** (2000) 2131

7. B. Paizs, J. Baker, S. Suhai and P. Pulay, *Geometry Optimization of Large Biomolecules in Redundant Internal Coordinates*,
    J. Chem. Phys. **113** (2000) 6566

8. I. Diaz-Acosta, J. Baker, W. Cordes and P. Pulay, *Calculated and Experimental Geometries and Infrared Spectra of Metal Tris-Acetylacetonates: Vibrational Spectroscopy as a Probe of Molecular Structure for Ionic Complexes. Part I*,
    J. Phys. Chem. A, **105** (2001) 238

9. P. Pulay and J. Baker, *Optimization and Reaction Path Algorithms*, in Encyclopedia of Chemical Physics and Physical Chemistry, to be published by IOP Press

10. S. Saebo and P. Pulay, *A Low-Scaling Mathod for Second-Order Moller-Plesset Calculations*, J. Chem. Phys. in press

11. J. Baker, R. Lopez-Boada and P. Pulay, *Expanding the Coulomb Potential in Spherical Harmonics: How High in L do we need to go for Accurate DFT Energies?* to be submitted